LOCALIZED RESONANCE OF COMPOSITE CORE-SHELL NANOSPHERES, NANOBARS AND NANOSPHE-RICAL CHAINS

Y.-F. Chau, Z.-H. Jiang, H.-Y. Li, G.-M. Lin, F.-L. Wu and W.-H. Lin

Department of Electronic Engineering
Ching Yun University, Jung-Li 320, Taiwan, R.O.C.

Abstract—We investigate the localized surface plasmon resonances (LSPR) of a pair of dielectric-core/silver-shell nanospheres, with and without a silver nanobar connecting them, for different values of the permittivity of the dielectric core, using the finite element method. Results show that the structure of a pair of core shells with a nanobar possesses a distinct blue-shifted behavior that can be manipulated from near infrared to visible light. The near field intensity can be enhanced by several orders of magnitude, and the working wavelengths depend on the shell thickness, dielectric medium in hollow metallic shell and the diameter of the nanobar. In addition, three or more pairs of nanospherical chain waveguides have also been investigated in our simulations.

1. INTRODUCTION

In recent years, plasmonic resonances in metallic systems [1–3] have attracted great interest due to their ability to change the light-matter interaction. It has been shown that the incident light interacting with nanometal can dramatically enhance the local electrical field by concentrating electromagnetic energy into sub-wavelength volumes [1]. This could lead to many potential applications, such as molecular specific imaging and spectroscopy [4], chemical and biological sensing [5], biomedicine [6] and nano-optical devices [7]. In addition, surface plasmon (SP) polaritons in thin metal shell have a direct implication in light and electron transmission across the shell [8, 9].

The lifetime of SP [10–13] has been demonstrated to strongly influence the field enhancement and the sensitivity of surface-enhanced Raman spectroscopy [14] and surface-enhanced fluorescence [15]. The use of plasmonic nanoparticles, such as metal nanorods or nanoshells, can tune the plasmon resonance to a wavelength longer than the onset for interband transitions [16].

The plasmonic properties of a nanostructure depend dramatically on its size and shape, as demonstrated in studies of nanorods [17], nanocubes [18], nanostars [19], nanoshells [20], and numerous other structures. An understanding of how the plasmonic properties depend on geometry enables the rational design of nanostructures tailored for specific applications such as surface enhanced spectroscopies [21], where one seeks to maximize the electromagnetic field enhancement over specific frequency ranges, or localized surface plasmon resonances (LSPR) sensing, where narrow spectral line widths and a high sensitivity to the dielectric environment are desirable [22].

Metal nanoshells, consisting of a dielectric core with a metallic shell of nanometer thickness, are a new, composite nanoparticle whose optical resonance can be designed in a controlled manner. By varying the relative dimensions of the core and shell, the optical resonance of these nanoparticles can be varied over hundreds of nanometers in wavelengths [23]. The nanoshells can be constructed by forming a hollow sphere inside the metallic nanosphere arrays or coating a metal thin film on the surface of the dielectric nanospheres. In recent years, the physical and chemical properties of metallic nanoshells have received particular attention [24–26]. Nanoshells possess several attractive features which make them interesting as nanoscale optical components. They possess a plasmon-derived tunable optical resonances controlled by the dimensions of a hollow sphere or dielectric medium in nanospheres and the thickness of metallic shell, spanning much of the visible and infrared regions of the optical spectrum [27, 28]. Additionally, nanoshells and other nanoscale metallic structures have been shown to greatly enhance local electromagnetic fields in certain regions near their surfaces at specific wavelengths of light, controlled by nanostructure geometry [29]. This subwavelength structure could functionally provide a tool for manipulating light below the diffraction limit.

Motivated by these previous works and based on our previous work [30], in this paper, we propose and demonstrate further improvements in the near field enhancements of two identical silver-shell nanospheres connected by a silver nanobar interacting with transverse magnetic (TM) mode incident plane wave by using the three-dimensional (3D) finite element method (FEM), which includes

the investigation of particle-particle interaction. The enclosure of a silver-shell nanospherical pair with dielectric cores (DCs) and a silver nanobar forms an open cavity model, and the electromagnetic field is effectively confined in the gap of the pair and the surface of a nanobar to generate an enhance local electromagnetic field. The refractive index of the DC, thickness of silver-shell nanosphere and the diameter of a silver nanobar play the key role and could endow additional variables to explore and tune the near field optical properties between the nanospherical pairs. We compared the optical response in near-field zone of silver-shell nanospherical pair with a solid silver counterparts. The influences of wavelength of incident light, shell-thickness, diameter of a silver nanobar and the refractive index in DCs on LSPR from our simulation results are discussed. Besides, near field optical response of three pairs and sixteen pairs of nanospherical chain waveguides has also been investigated in this paper

2. SIMULATION METHOD

The simulations in this work have been done in the quasistatic regime. Quasi-static implies that spatially the field is static, i.e., no retardation effect, but temporally oscillates according to $\exp[i\omega t]$. The quasi-static approximation [24] can be employed when the diameter of nanoparticle is much smaller than the wavelength.

The dispersion properties of the metal must be considered here since the absorption and permittivity of the metallic material are frequency dependent. Throughout this paper we consider solid-silver and silver-shell nanospherical pair and use the experimental data from Johnson and Christy [31] for the permittivity, $\varepsilon(\lambda)$, as a function of the wavelength λ. The Drude model [32–35] represents the dispersive dielectric response, $\varepsilon(\omega)$, of the silver particles, i.e.,

$$\varepsilon(\omega) = \varepsilon_\infty - \frac{\omega_p^2}{\omega(\omega + i\Gamma_D)} \tag{1}$$

The Drude model parameters in Equation (1), namely the dielectric function of the core electrons of the metal, ε_∞, the angular plasma frequency for free electrons, ω_P, and the intrinsic damping parameter, Γ_D, are obtained by fitting on the Johnson and Christy [31] optical bulk experimental data for the frequency region of interest. Data for the plasma frequency and Drude damping parameter for silver can be taken from the graphs and tables in [34, 35].

In our simulations, we used 3D FEM [36, 37] with triangular high order edge elements. To model an infinite simulation region with a 3D finite-geometry model (i.e., to enclose the computational

domain without affecting the numerical solution), it is necessary to use anisotropic perfectly matched layers (PMLs) [36–38] that are placed before the outer boundary. This formulation can be used to deal with anisotropic material in terms of both dielectric permittivity and magnetic permeability, allowing anisotropic PMLs to be implemented directly.

3. RESULTS AND DISCUSSION

Metallic nanoshells possess optically excitable plasmon resonances that can be tuned throughout the visible and into the infrared regions of the electromagnetic spectrum by changing their aspect ratio, r_1/r_2, where r_1 and r_2 are the inner and outer radii of the metallic shell layer, and $r_1 - r_2$ is the metal shell thickness [17]. In this case, the metal shell of the individual nanoparticle controls its plasmon resonance, thus controlling its local electromagnetic field. The LSPRs response of individual nanoshells covered with nonresonant molecules has been shown to be a function of their aspect ratio [24]. Thus, the metal shell thickness represents the distance over which this interaction takes place, and this interaction refers to LSPR.

A pair of close metal nanoparticles provides a stronger electric field in the gap region than a single metallic nanoparticle does in its proximity; meanwhile, a pair of metallic nanoshell particles can provide a stronger local electric field than a single nanoshell and/or a pair of solid metallic nanoparticles [20]. The plasmon coupling strength between the core (air or dielectric medium inside the DC) and sphere-shell modes vanishes over the size of shell thickness similar to the decay of the plasmonic field in the interparticle gap of the particle-pair system. Compared to a solid metallic nanospherical pair which is no DC inside the DH, there is no plasmonic core mode as the core is filled with metal.

Firstly, the difference of near field optical response and LSPR on a solid-silver pair and a silver-shell nanospherical pair with a different refractive medium in a pair of hollow metallic shells is investigated to understand the roles of the particle-particle interaction. For convenience, we name the case of two identical solid-silver nanospheres as a pair of solid silver spheres [see Figure 1(a)] and the case of two identical silver-shell nanospheres with dielectric medium in nanospheres [see Figure 1(b)] as DC case. We compare the near field optical response of a pair of solid silver spheres with DC case. The simulation models are illuminated with a TM electromagnetic plane wave and propagated in the k direction. The wavelength of incident light varies from 350 nm to 800 nm. The gap (interparticle distance)
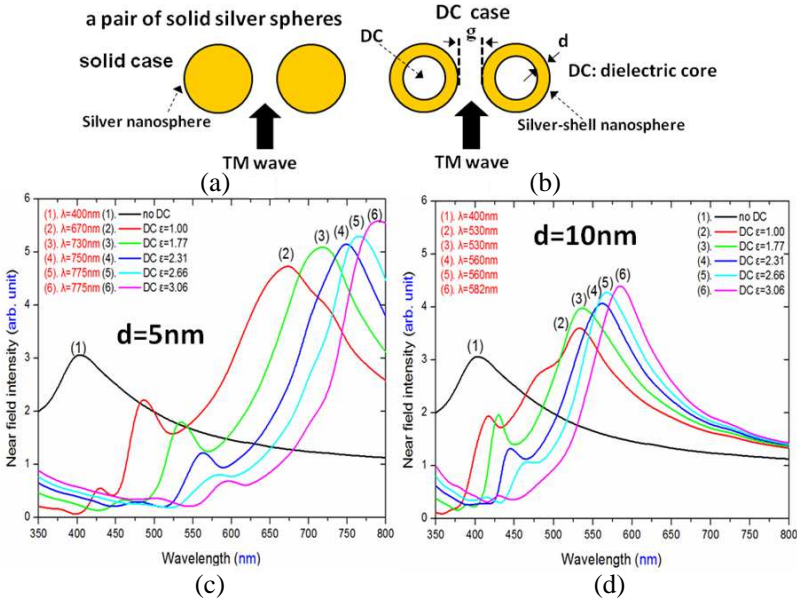
Figure 1. (a) A pair of solid silver spheres. (b) A pair of silver-shell nanospheres with dielectric cores in nanospheres (DC cases), near field intensities of a pair of solid silver spheres and DC cases with different shell thickness, i.e., (c) $d = 5$ nm and (d) 10 nm, and different medium in DCs as a function of wavelengths of TM incident light.

is set to $g = 20$ nm, and the near field intensity is measured in the central part of the gap. Near field intensities of local fields in the gaps between a pair of solid silver spheres and DC cases are also quite sensitive to the radii of the nanospheres. In the nanoshell system, we can expect the fractional shift of the dipolar resonance to be a function of $(d/r_2 + 1)^{-3}$, where $d = r_1 - r_2$ is the shell thickness; r_1 is the radius of solid-silver nanospherical pair; and r_2 is the core radius of silver-shell nanosphere. In other words, a larger core has a larger polarizability, and a thinner shell ensures stronger near field coupling, thus leading to a larger fractional plasmon shift. In fact, the dipolar resonance condition for a core-shell structure in the quasistatic limit is specified by [39–41]:

$$\varepsilon_c = -2\varepsilon_s \frac{\varepsilon_s(1-f) + \varepsilon_m(2+f)}{\varepsilon_s(1+2f) + 2\varepsilon_m(1-f)} \tag{2}$$

where ε_c, ε_s and ε_m are the dielectric constants of the silver-shell nanospheres, the silver shell, and the dielectric core, respectively, and f is the fraction of the volume of the core in the composite structure.

It is interesting to note that f is essentially $(d/r_2 + 1)^{-3}$. This analogy serves to qualitatively explain the similarity of the distance dependence and scaling behavior of plasmon coupling in the nanoshell structure to that in the particle-pair structure. On the basis of our simulations, we set the radius $r_1 = 50$ nm in a pair of solid silver spheres, and the outer and inner radii of $r_1 = 50$ nm and $r_2 = 40, 45$ nm (i.e., $d = 10$ nm, 5 nm) in DC case, respectively.

The coupling between the nanoparticles influences the corresponding charge distribution: The charge density is more concentrated on the sides of the gap between the nanospherical pair than on the external sides [8, 9, 20]. Turning to the DC case with a refractive medium in the DCs, we have another variable ε_c to explore the near field optical properties. The silver-shell nanospherical pair is a unique shape of the nanoparticles; it is empty inside and has holes on its walls to allow molecules to absorb on the inside surface of the walls as well as on the outside. This could be due to the symmetric distribution of positive and negative charges on the surface of inside and outside the shells, which can induce the dipole resonance. Furthermore, the dipole moments of the inner and outer surfaces are aligned. There is a strong electromagnetic coupling between the inner and outer shell walls when the thickness $d = r_1 - r_2$ is small compared to the nanosphere radius r_1. This leads to a new scheme of polarization and results in mode splitting similar to the case of a thin metallic slab, which is characterized by symmetric and antisymmetric mode branches [42, 43].

Figures 1(c) and (d) show the near field intensities of a pair of solid silver spheres and a DC case with different shell thicknesses ($d = 5$ nm and 10 nm) and different media in DCs as a function of wavelengths of TM incident light. For certain modes the peak positions are given under the resonant waves and for others are not given under the off-resonant wave. In Figures 1(c) and (d), an evident difference on optical properties is observed between the solid case and DC case. One can recognize one resonance peak in solid case and three resonances in DC case. The first one is due to high frequency (short wavelength) oscillation between nanospheres and incident light. The second one of DC case results from interaction of the two identical silver-shell nanospheres. In a metallic nanoshell there appear two dipole modes due to plasmon hybridization [44]. Actually, all multipole modes can in principle be excited, though those with long lifetimes are washed out by absorption [10]. The shift of the major resonance peak of DC cases visible in Figures 1(c) and (d) exhibits that increasing of the dielectric constant (ε) in DCs results in a higher near field intensity and the red-shift trend with the increasing ε. This phenomenon can be explained in combination with the SPR on nanoshell and the

refractive medium in DCs. The performance of different silver-shell thicknesses on near field intensity is also illustrated in Figures 1(c) ($d = 5$ nm) and (d) ($d = 10$ nm), which shows that a very different behavior depending on the shell thickness is observed. Note that all the resonance peaks broaden and the near field intensities enhance as the size of shell thickness decreases from $d = 10$ nm [Figure 1(d)] to $d = 5$ nm [Figure 1(c)]. It can be seen from Figures 1(c) and (d) that the peak wavelengths in DC cases are in the range of 670–775 nm for case $d = 5$ nm and 530–582 nm for case $d = 10$ nm. A distinct blue-shifted behavior depending on the shell thickness is observed, i.e., the working peak wavelengths can be manipulated from near infrared to visible light by decreasing d and ε in DC case.

The top of Figure 2 depicts that the positive and negative charges accumulate on the side of the gap and that the charge density is more concentrated on the sides of the gap between the particle-pairs than on the external sides. Additional positive and negative charges accumulated on the nanobar (with a diameter of w) can be found on the top of Figure 2(b). One can expect that the use of two identical solid-silver nanospheres connected by a silver nanobar may provide additional positive-negative charge pairs between the gap compared to the same structure but without a nanobar. Figures 2(a) and (b) show the near-field distribution corresponding to the models shown on the top of Figures 2(a) and (b). A stronger near field distribution concentrated between the gap of nanospherical pair in Figure 2(b) than that of Figure 2(a) is due to the fact that the additional positive-negative charge-pairs on the surface of the nanobar which can induce more dipole-dipole interaction in the hot spot region (gap).
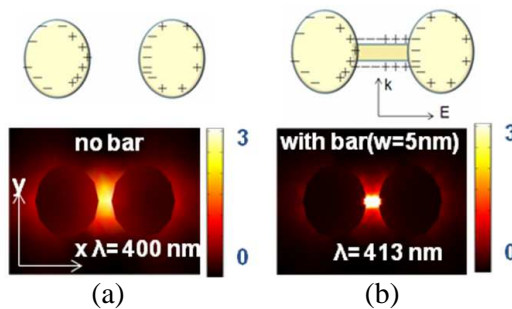
Figure 2. Near-field distribution corresponding to the models shown on the top of these figures at their corresponding resonant peak wavelengths. (a) No bar case ($\lambda = 400$ nm), (b) with bar case ($\lambda = 413$ nm).

Now we investigate the difference of LSPR on a solid case connected by a silver nanobar [Figure 3(a), we name it as case 1] and the DC cases connected by a silver nanobar [Figure 3(b), we name it as case 2] with different diameters of silver nanobar (w) and shell thicknesses (d), which is illuminated with a TM electromagnetic plane wave. The positive-negative charge distributions are illustrated in Figure 3(c). Three different diameters of silver nanobar are examined, i.e., $w = 2.5$, 5 and 10 nm, respectively. The gap is set to $g = 20$ nm. From Figure 3, a clear LSPR can be found as w is less than 10 nm. Because the light is absorbed by more volume of metal in the gaps, the intensity of LSPR is decreased as w is larger than 10 nm.
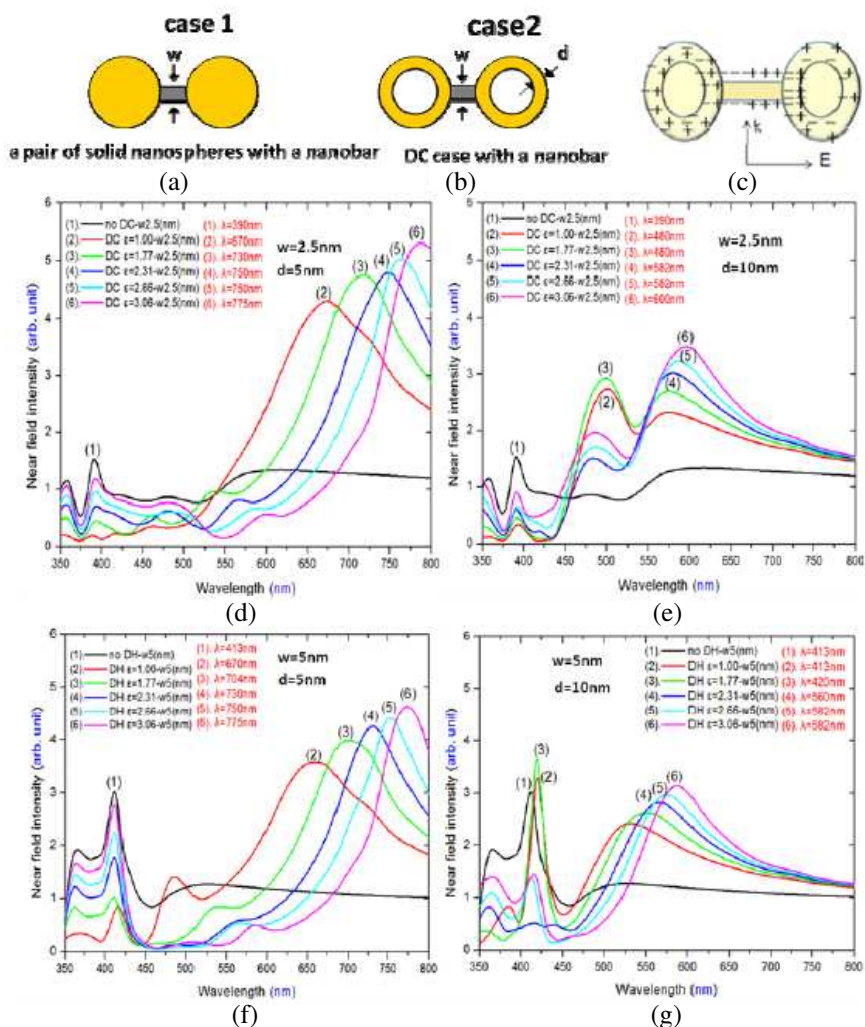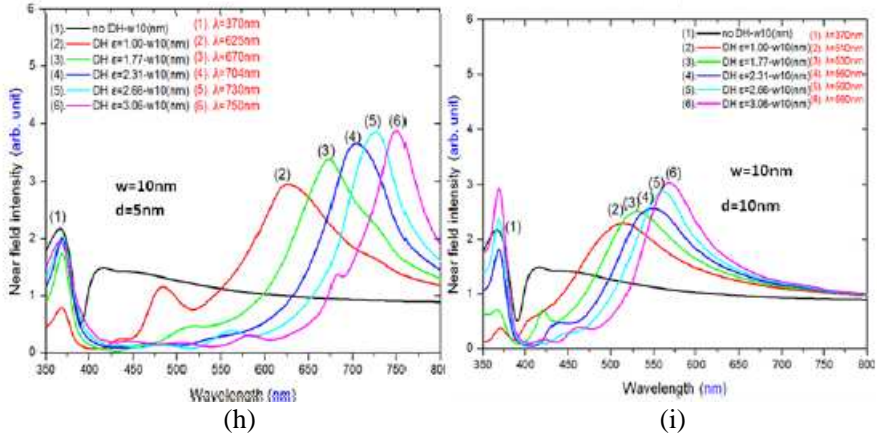
Figure 3. (a) Case 1, (b) case 2, (c) charge distribution of case 2, (d)–(i) difference of near-field intensities of case 1 and case 2 with different w and d.

From Figures 3(d)–(i), two clear resonance peaks in the range of $\lambda = 350$–450 nm for case 1 and four pronounced resonance peaks in the range of $\lambda = 350$–800 nm (ultraviolet-visible-near infrared) for cases 2 can be found. The second resonance peak for case 2 is the shifted single nanoparticle dipole resonance, and the shift is due to dipole-dipole interaction. The other resonance peaks are attributed to the effect of a silver nanobar interacted with the incident light. One can observe the case 2 in Figure 3 that the performance of shell thickness of $d = 5$ nm [Figures 3(d), (f) and (h)] is quite different from that of $d = 10$ nm [Figures 3(e), (g) and (i)] and can be designed by varying the width of nanobar ($w = 10$, 5 and 2.5 nm) and exhibits two physically different types of resonances: (1) for the cases of $d = 5$ nm, remarkably enhance the near field intensity by decreasing the width of nanobar, and (2) for the cases of $d = 10$ nm, remarkably blue-shift the LSPR by increasing the width of nanobar. Compared to the same cases but without the nanobar as shown in Figures 1(a) and (b), a very distinct LSPR can be found near the ultraviolet ($\lambda = 350$–450 nm) for all cases. For small diameter of nanobar ($w = 2.5$ and 5 nm), two enhancing peak values associated with the interaction of nanoparticle pair and the nanobar is visible. Note that four distinct peak wavelengths can be obtained for case with $w = 2.5$ nm and $d = 10$ nm at $\lambda = 350$, 390, 480 and 600 nm, respectively, as illustrated in Figure 3(e).

In order to realize the detailed behaviors of the field distribution inside the case 2, the three components of the field distribution will be discussed here. To find the contribution of LSPRs, we plot the

polarization components of the field. The polarized incident wave is enhanced in case 2 and decayed gradually after exiting the end of case 2, producing two perpendicularly polarized electric field components — that is, the incident field is entirely polarized along the x axis and the scattered field also has components along the y and z axes, respectively. These components produce depolarization at this interface around case 2. A more detailed calculation using the 3D FEM is shown in Figure 4, which illustrates the near field distribution obtained at x-y sectional plane at $z = 0$ with different dielectric constants in DCs. From top to bottom, Figure 4 illustrates the case of $w = d = 5$ nm and shows the TM-mode near-field distributions of three components E_x, E_y, and E_z and total field distribution E_t. Figure 4 shows the near field distribution at the resonance wavelength for different dielectric constants. The corresponding TM-mode near field distributions of three components (E_x, E_y, and E_z) and total field (E_t) are (a) $\lambda = 670$ nm for $\varepsilon = 1$ (a hollow sphere), (b) $\lambda = 704$ nm for $\varepsilon = 1.77$, (c) $\lambda = 730$ nm for $\varepsilon = 2.31$, (d) $\lambda = 750$ nm for $\varepsilon = 2.66$ and (e) $\lambda = 775$ nm for $\varepsilon = 3.06$. From the results of Figure 4, we find that with the 50 nm diameter of a silver-shell nanospherical pair connected by a nanobar, a larger number of LSPRs can be excited, which interact with the incident field and form the localized field enhancement. This is to be expected because many surface charge densities will be induced
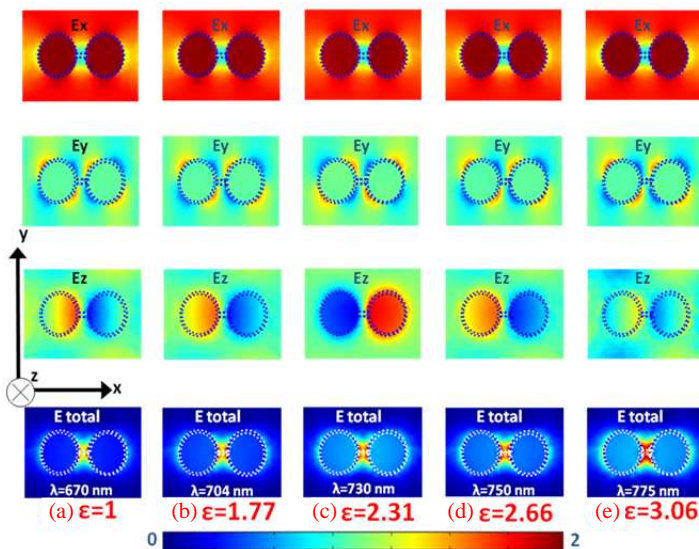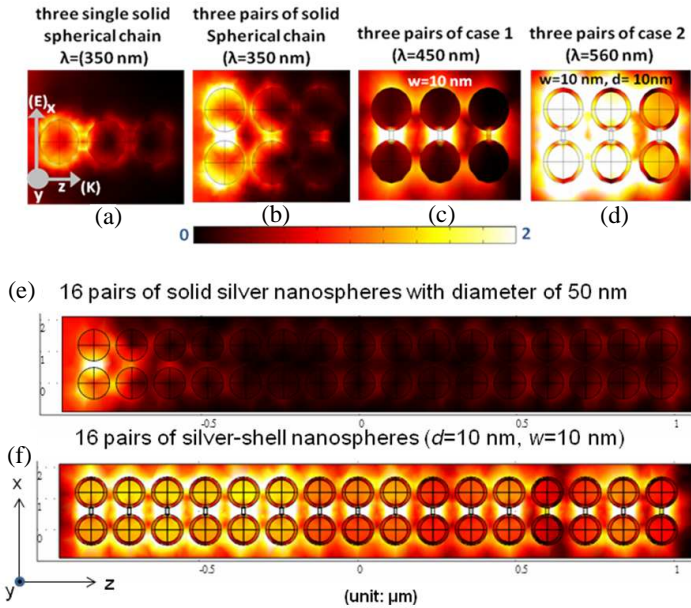

Figure 4. TM-mode near-field distributions of three components E_x, E_y, and E_z and total field distribution E_t for the case of $w = d = 5$ nm.

in the circumference around the inside and outside of case 2 [see Figure 3(c)] by the incident electric fields. The strongest field intensity (peak value) is found at the gap of case 2. Note that the local field at the circumference of the silver-shell nanospherical pair and the surface of the nanobar extends in the tens of nanometers range from case 2. The field enhancement of case 2 originates mainly from the LSPR mode excited by the evanescent field.

Silver-shell nanosphere with a nanobar is a new hybrid nanoparticle geometry that combines the intense local fields of nanospheres with the highly tunable plasmon resonances of nanoshells [44]. The highly tunable LSPR essentially arise from plasmon hybridization among a pair of silver-shell nanospheres, a pair of spherical nanocavity or dielectric medium inside the spherical pair, and a nanobar. The excitation of the nanosphere plasmon gives rise to enormous local field enhancements exploitable for surface-enhanced Raman spectroscopy (SERS). The plasmon resonance frequency of nanosphere is extremely sensitive to surrounding dielectric media, holding great potential for monitoring localized environmental changes during chemical and biological processes.

From the analysis and discussion of the above cases, we can summarize that highly efficient LSPRs can be achieved in a silver nanospherical pairs connected by a silver nanobar through a proper design of the shell thickness (d), dielectric constant (ε) in DCs and the diameter of the silver nanobar (w). The near field intensity can be enhanced by several orders of magnitude and the resonance of the spectrum depends on ε, d and w. As deduced from the previous simulation results, now we investigate the transmission properties of chain waveguides made of case 2. One commonly used approach for evaluating the transmission properties of a chain waveguide is to use the SNOM tip to drive the first particle at the near end of the chain [45–47]. The energy transport in the chain is then realized by the field coupling between the modes of the neighboring particles [45, 46]. The propagation length is determined based on the energy decay within the particle chain. In the end of this work, we will focus mainly on the cases when the chains are driven at the resonances of two identical silver-shell nanospheres connected by a silver nanobar as discussed above.

Figures 5(a)–(f) compare the near field intensity at their corresponding peak wavelengths for the chain waveguides with (a) a chain of three solid silver spheres, (b) a chain of three pairs of solid silver spheres, (c) three pairs of case 1 ($w = 10$ nm), (d) three pairs of case 2 ($w = d = 10$ nm), (e) a chain of 16 pairs of solid silver spheres and (f) 16 pairs of case 2, respectively. The chain waveguides are illuminated with a TM electromagnetic plane wave along the chain

Figure 5. Near field distributions at their corresponding peak wavelengths for the chain waveguides with (a) a chain of three solid silver spheres, (b) a chain of three pairs of solid silver spheres, (c) three pairs of case 1, (d) three pairs of case 2, (e) a chain of 16 pairs of solid silver spheres and (f) 16 pairs of case 2, respectively.

axis, and their parameters are shown in the inset of Figure 5. From the field distributions as shown in Figure 5, one can observe that the mesoscopic nature of the finite chain waveguide is clearly visible, as the near field intensity of case 1 [Figure 5(c)] dramatically enhance the near field intensities in the gap with the connection of a silver nanobar, e.g., compared to a chain of three solid silver spheres [see Figure 5(a)] and three pairs of solid silver spheres which is without a silver nanobar [see Figure 5(b)]. Turning to case 2 which has silver nanobars connected between two identical silver-shell nanospheres as shown in Figure 5(d), the field is well confined effectively not only along the surface of the silver-shell nanospheres, but also on the surface of the silver nanobars. It can also be demonstrated from Figures 5(e) and (f) that the near field intensities of more pairs of case 2 can dramatically enhance the near field along the chain axis. Figures 5(e) and (f) compare the near field distributions of 16 pairs of solid silver spherical chain and 16 pairs of case 2, respectively. It can be verified that our proposed case 2 structure is pertinent to the functionality of long range of wave guiding

($> 2\,\mu\text{m}$) or other optical devices. The field enhancement of the silver nanospherical pair originates mainly from the localized surface plasmon mode excited by the evanescent field.

4. CONCLUSION AND OUTLOOK

In conclusion, we have investigated LSPR of a pair of core-shell silver-nanospheres connected by a silver nanobar with different dielectric cores (DCs) using FEM. Results show that the proposed structure exhibit tunable plasmon resonances that are not observed for a solid case of the same size. The proposed case 2 structure possesses a distinct blue-shifted behavior, i.e., the working wavelengths can be manipulated from near infrared to visible light by varying ε, w and d. It can also be demonstrated that the more pairs (16 pairs) of the proposed case 2 structure can dramatically enhance the near field intensities along the chain axis ($> 2\,\mu\text{m}$). The volume confined by two identical silver-shell nanospheres connected by a nanobar with refractive medium in DCs is accessible to various sensing and spectroscopy applications at the nanometer scale. As observed from numerical simulations, the main features can be qualitatively understood from a simple silver-shell nanospherical pair with a nanobar model. Silver-shell nanospherical pairs could serve as resonant nanocavities to hold and probe smaller nanostructures, such as biomolecules or quantum dots. The predictive character of these calculations allows one to tailor the morphological properties of the nanoparticle to achieve excitation spectra on demand with a controlled field enhancement. Our proposed case 2 structure also shows promise for applications in nanooptical devices, sensing, and surface-enhanced spectroscopy, due to the effects of strong and tunable plasmon resonance.

In the end of this paper, we will briefly discuss the nonlocal effects which are very prominent for small structure [48–50], when describing metal-light interactions at the nanometer length scale. In such systems, it is necessary to consider the reduced mean free path of the sp-band electrons due to electron-interface scattering. Recently, McMahon et al. have studied the optical properties of arbitrarily shaped structures (including spherical nanoparticles) and demonstrated the longitudinal plasmons characteristic of nonlocal effects [48]. They demonstrated a number of effects that result from the spatial nonlocality in the dielectric response, including anomalous absorption, blueshifting of LSPRs, and decreases in electromagnetic field enhancements. In the future, we plan to consider nonlocal calculations, which will allow even more accurate descriptions of nonlocal optical phenomena than those presented in this work.

ACKNOWLEDGMENT

REFERENCES

1. Wang, F. and Y. R. Shen, "General properties of local plasmons in metal nanostructures," *Phys. Rev. Lett.*, Vol. 97, 206806, 2006.

2. Politano, A., V. Formoso, and G. Chiarello, "Dispersion and damping of gold surface plasmon," *Plasmonics*, Vol. 3, 165–170, 2008.

3. Ozbay, E., "Plasmonics: Merging photonics and electronics at nanoscale dimensions," *Science*, Vol. 311, 189–193, 2006.

4. El-Sayed, I. H., X. Huang, and M. A. El-Sayed, "Surface plasmon resonance scattering and absorption of anti-egfr antibody conjugated gold nanoparticles in cancer diagnostics: Applications in oral cancer," *Nano Lett.*, Vol. 5, 829–834, 2005.

5. Haes, A. J., S. Zou, G. C. Schatz, and R. P. Van Duyne, "Nanoscale optical biosensor: Short range distance dependence of the localized surface plasmon resonance of noble metal nanoparticles," *J. Phys. Chem. B*, Vol. 108, 6961–6968, 2004.

6. Loo, C. A., A. Lowery, N. Halas, J. West, and R. Drezek, "Immunotargeted nanoshells for integrated cancer imaging and therapy," *Nano Lett.*, Vol. 5, 709–711, 2005.

7. Mirin, N. A., K. Bao, and P. Nordlander, "Fano resonances in plasmonic nanoparticle aggregates," *J. Phys. Chem. A*, Vol. 113, 4028–4034, 2009.

8. Andrew, A. and W. L. Barnes, "Energy transfer across a metal film mediated by surface plasmon polaritons," *Science*, Vol. 306, 1002–1005, 2004.

9. Okamoto, K., I. NiKi, A. Scherer, Y. Narukawa, and T. Mukai, "Surface-plasmon-enhanced light emitters based on InGaN quantum wells," *Nature Mater.*, Vol. 3, 601–605, 2004.

10. Politano, A. and G. Chiarello, "Tuning the lifetime of the surface plasmon upon sputtering," *Phys. Status Solidi-Rapid Res. Lett.*, Vol. 3, No. 5, 136–138, 2009.

11. Pinchuk, A. and U. Kreibig, "Interface decay channel of particle surface plasmon resonance," *New J. Phys.*, Vol. 5, 151.1–151.15, 2003.

12. Ishida, H. and A. Liebsh, "Lifetime of surface plasmons of simple metals: Volume versus surface contributions," *Phys. Rev. B*, Vol. 54, 14127, 1996.

13. Yuan, Z. and S. Gao, "Landau damping and lifetime oscillation of surface plasmons in metallic thin films studied in a jellium slab model," *Surf. Sci.*, Vol. 602, 460–464, 2008.

14. Nie, S. and S. R. Emory, "Probing single molecules and single nanoparticles by surface-enhanced. Raman scattering," *Science*, Vol. 275, 1102–1106, 1997.

15. Sokolov, K., G. Chumanov, and T. Cotton, "Among Ag, Al and Au layers, the emission intensity of YAG: Ce thin-film phosphor by coating a silver," *Anal. Chem.*, Vol. 70, 3898–3905, 1998.

16. Lassiter, J. B., J. Aizpurua, L. I. Hernandez, D. W. Brandl, I. Romero, S. Lal, J. H. Hafner, P. Nordlander, and N. J. Halas, "Close encounters between two nanoshells," *Nano Lett.*, Vol. 8, 1212–1218, 2008.

17. Chau, Y.-F., H.-H. Yeh, and D. P. Tsai, "Near-field optical properties and surface plasmon effects generated by a dielectric hole in a silver-shell nanocylinder pair," *Appl. Opt.*, Vol. 47, 5557–5561, 2008.

18. Sun, Y. and Y. Xia, "Shape-controlled synthesis of gold and silver nanoparticles," *Science*, Vol. 298, 2176–2179, 2002.

19. Nehl, C. L., H. Liao, and J. H. Hafner, "Optical properties of star-shaped gold nanoparticles," *Nano Lett.*, Vol. 6, 683–688, 2006.

20. Chau, Y. F., H. H. Yeh, and D. P. Tsai, "Surface plasmon resonances effects on different patterns of solid-silver and silver-shell nanocylindrical pairs," *Journal of Electromagnetic Waves and Applications*, Vol. 24, Nos. 8–9, 1005–1014, 2010.

21. Talley, C. E., J. B. Jackson, C. Oubre, N. K. Grady, C. W. Hollars, S. M. Lane, T. R. Huser, P. Nordlander, and N. J. Halas, "Surface-enhanced raman scattering from individual au nanoparticles and nanoparticle dimer substrates," *Nano Lett.*, Vol. 5, 1569–1574, 2005.

22. Sherry, L. J., S.-H. Chang, G. C. Schatz, R. P. V. Duyne, B. J. Wiley, and Y. Xia, "Localized surface plasmon resonance spectroscopy of single silver nanocubes," *Nano Lett.*, Vol. 5, 2034–2038, 2005.

23. Oldenburg, S. J., R. D. Averitt, S. L. Westcoot, and N. J. Halas, "Nanoengineering of optical resonances," *Chem. Phys. Lett.*, Vol. 288, 243–247, 1998.

24. Lassiter, J. B., J. Aizpurua, L. I. Hernandez, D. W. Brandl,

I. Romero, S. Lal, J. H. Hafner, P. Nordlander, and N. J. Halas, "Nanoshells dimers and overlapped dimmers," *Nano Lett.*, Vol. 8, 1212–1218, 2008.

25. Jain, P. K. and M. A. El-Sayed, "Scaling of plasmon coupling in nanoshells," *Nano Lett.*, Vol. 7, 2854, 2007.

26. Brandl, D. W., C. Oubre, and P. Nordlander, "Plasmon hybridization in nanoshell dimmers," *J. Chem. Phys.*, Vol. 123, 024701, 2005.

27. Tserkezis, C., G. Gantzounis, and N. Stefanou, "Collective plasmonic modes in ordered assemblies of metallic nanoshells," *J. Phys.: Condens. Matter*, Vol. 20, 075232, 2008.

28. Hu, Y., R. C. Fleming, and R. A. Drezek, "Optical properties of gold-silica-gold multilayer nanoshells," *Opt. Express*, Vol. 16, 19579–19591, 2009.

29. Averitt, R., D. Sarkar, and N. Halas, "Plasmon resonance shifts of Au-coated Au2S nanoshells: Insight into multicomponent nanoparticle growth," *Phys. Rev. Lett.*, Vol. 78, 4217–4220, 1997.

30. Chau, Y.-F., "Surface plasmon effects excited by the dielectric hole in a silver-shell nanospherical pair," *Plasmonics*, Vol. 4, 253, 2009.

31. Johnson, P. B. and R. W. Christy, "Optical constants of the noble metals," *Phys. Rev. B*, Vol. 6, 4370–4379, 1972.

32. Zhang, R., S. Dods, and P. Catrysse, "FDTD approach for optical metallic material," *Laser Focus World*, Vol. 68, 2004 (www.laserfocusworld.com).

33. Veronis, G., R. W. Dutton, and S. Fan, "Metallic photonic crystals with strong broadband absorption at optical frequencies over wide angular range," *J. Appl. Phys.*, Vol. 97, No. 9, 2005.

34. Ordal, M. A., L. L. Long, R. J. Bell, S. E. Bell, R. R. Bell, R. W. Alexander, Jr., and C. A. Ward, "Optical properties of the metals Al, Co, Au, Fe, Pb, Ni, Pd, Pt, Ag, Ti, and W in the infrared and far infrared," *Appl. Optics*, Vol. 22, 4493–4499, 1983.

35. Ordal, M. A., R. J. Bell, R. W. Alexander, Jr., L. L. Long, and M. R. Querry, "Optical properties of the metals Al, Co, Au, Fe, Pb, Ni, Pd, Pt, Ag, Ti, and W in the infrared and far infrared," *Appl. Optics*, Vol. 24, 1099–1120, 1985.

36. Gresho, P. M. and R. L. Sani, *Incompressible Flow and Finite Element Method*, Vol. 1 & 2, John Wiley and Sons, New York, 2000.

37. Monk, P., *Finite Element Methods for Maxwell'S Equations*, 85, Clarendon, Oxford, 2003.

38. Okamoto, T., *Near-field Optics and Surface Plasmon Polaritons*, 99, S. Kawata (Ed.), Springer, Berlin, 2001.

39. Bohren, C. F. and D. R. Huffman, *Absorption and Scattering of Light by Small Particles*, Wiley, New York, 1983.

40. Jain, P. K. and M. A. El-Sayed, "Universal scaling of plasmon coupling in metal nanostructures: Extension from particle pairs to nanoshells" *Nano Lett.*, Vol. 7, 2854–2858, 2007.

41. COMSOL Multiphysics 4.1 TM, http://www.comsol.com.

42. Prodan, E., C. Radloff, N. J. Halas, and P. Nordlander, "A hybridization model for the plasmon response of complex nanostructures," *Science*, Vol. 302, 419, 2003.

43. Teperik, T. V., V. V. Popov, and F. J. Garcia de Abajo, "Radiative decay of plasmons in a metallic nanoshell," *Phys. Rev. B*, Vol. 69, 155402, 2004.

44. Wang, H., D. W. Brandl, P. Nordlander, and N. J. Halas, "Tunable plasmonic nanostructures: From fundamental nanoscale optics to surface-enhanced spectroscopies," *Acc. Chem. Res.*, Vol. 40, 53–62, 2007.

45. Ditlbacher, H., J. R. Krenn, G. Schider, A. Leitner, and F. R. Aussenegg, "Two-dimensional optics with surface plasmon polaritons," *Appl. Phys. Lett.*, Vol. 81, 1762–1764, 2002.

46. Maier, S. A., P. G. Kik, H. A. Atwater, S. Meltzer, E. Harel, B. E. Koel, and A. A. G. Requicha, "Local detection of electromagnetic energy transport below the diffraction limit in metal nanoparticle plasmon waveguides," *Nat. Mater.*, Vol. 2, 229–232, 2003.

47. Cui, X. and D. Erni, "Enhanced propagation in a plasmonic chain waveguide with nanoshell structures based on low- and high-order mode coupling," *J. Opt. Soc. Am. A*, Vol. 25, 1783–1789, 2008.

48. McMahon, J. M., S. K. Gray, and G. C. Schatz, "Calculating nonlocal optical properties of structures with arbitrary shape," *Phys. Rev. B*, Vol. 82, 035423, 2010.

49. Tserkezis, C., G. Gantzounis, and N. Stefanou, "Collective plasmonic modes in ordered assemblies of metallic nanoshells," *J. Phys.: Condens. Matter*, Vol. 20, 075232, 2008.

50. Yannopapas, V., "Non-local optical response of two-dimensional arrays of metallic nanoparticles," *J. Phys.: Condens. Matter*, Vol. 20, 325211, 2008.